IIETA International Information and Engineering Technology Association
Advancing the World of Information and Engineering

International Journal of Design & Nature and Ecodynamics
Vol. 21, No. 8, August, 2026, pp. 2247-2258
Journal homepage: http://iieta.org/journals/ijdne

Comparative Estimation and Spatial Distribution Mapping of Total Suspended Solids Using Four Empirical Algorithms and Sentinel-2 Level-2A Imagery in the Downstream Krueng Aceh Watershed, Indonesia: A Single-Date Assessment in 2025

Ichwana Ramli[1,2*], Rusli Yusuf[3], Miftahuddin[4], Afdhalul Aulia[2], Athiya Iffaty[5], Addyat Amal[5]

[1] Master Program of Environmental Management, Graduate School, Syiah Kuala University, Banda Aceh 23111, Indonesia
[2] Department of Agricultural Engineering, Faculty of Agriculture, Syiah Kuala University, Banda Aceh 23111, Indonesia
[3] Department of Civic Education, Faculty of Teacher Training and Education, Syiah Kuala University, Banda Aceh 23111, Indonesia
[4] Department of Statistics, Faculty of Mathematics and Sciences, Syiah Kuala University, Banda Aceh 23111, Indonesia
[5] Department of Urban and Regional Planning, Universitas Diponegoro, Semarang 50265, Indonesia

Corresponding Author Email: ichwana.ramli@usk.ac.id

https://doi.org/10.18280/ijdne.210807

Received: 15 June 2026
Revised: 19 August 2026
Accepted: 26 August 2026
Available online: 31 August 2026

Keywords:
Total Suspended Solids, Sentinel-2 Level-2A, empirical algorithms, water quality, remote sensing, Krueng Aceh, single-date assessment

ABSTRACT

Total Suspended Solids (TSS) is an important indicator of water quality and sediment dynamics in river systems. This study compared four published empirical algorithms, namely Liu, Laili, Budhiman, and Parwati, for estimating TSS using Sentinel-2 Level-2A imagery in the downstream Krueng Aceh watershed, Indonesia. Field sampling was conducted at ten observation points on 26 August 2025, and TSS concentrations were measured using the gravimetric method according to SNI 6989.3:2019. Sentinel-2C Level-2A imagery acquired on the same date was processed using cloud and cloud-shadow masking, Normalized Difference Water Index (NDWI)-based water extraction, and spectral reflectance extraction using a 3 × 3 pixel mean window. The published algorithms were applied using their original coefficients without recalibration. Leave-one-out cross-validation (LOOCV) was used to assess performance stability under the limited sample size. Under LOOCV, Laili produced the lowest RMSE (1.5163 mg/L) and MAPE (16.1822%), while Liu produced the highest R^2 (0.1126). Laili showed an R^2 of 0.0670, indicating limited predictive ability. Budhiman and Parwati produced negative R^2 values of -0.5376 and -0.3084, respectively. Although non-cross-validated results showed better apparent performance, particularly for Laili, these values should not be interpreted as robust predictive accuracy. Overall, Laili showed the best relative performance but limited predictive ability. Larger multi-season datasets and independent validation are required for reliable operational TSS monitoring.

1. INTRODUCTION

Water quality reflects the condition of a water body and its suitability for supporting human needs and ecosystem sustainability. In general, water quality parameters are grouped into three main categories, namely physical, chemical, and biological parameters, each of which plays an important role in assessing the characteristics and ecological functions of water bodies [1].

TSS is an important parameter that is used to assess water quality by indicating the concentration of suspended particles. In the past couple of decades, remote sensing has become a key tool for comprehensive environmental monitoring. The use of satellite imagery enables broad spatial observation and continuous analysis of environmental parameters, which is particularly important in coastal and estuarine areas. One of the most widely used remote sensing systems is Sentinel-2. This satellite provides multispectral data with high spatial resolution (up to 10 meters in some bands). Sentinel-2 captures the light spectrum from visible to near-infrared, which is highly sensitive to changes in suspended particle content in water [2].

Human activities along the Krueng Aceh watershed area, such as agriculture, settlement, and infrastructure development, have worsened the sedimentation and water turbidity problem. This reduces water clarity, inhibits light penetration for photosynthesis by aquatic organisms, and accelerates river siltation. Downstream areas such as the Krueng Aceh estuary are vulnerable to flooding and water quality degradation, especially in areas adjacent to markets and landfills [3]. Increasing population growth leads to higher water resource demand, highlighting the importance of water resource management that considers environmental carrying capacity [4]. In addition to land-use and urban activities, wastewater and leachate inputs may also contribute to local variations in water quality. Previous monitoring at the Blang Bintang landfill reported a decline in water quality in the Krueng Uteun Siblah River immediately downstream of the leachate outfall, with increased BOD, COD, and Fe concentrations and decreased dissolved oxygen levels [5].

Remote sensing offers substantial advantages over traditional monitoring methods, especially due to the synoptic coverage and temporal consistency of the data, and has the potential to provide important information about inland transitional waters and near coastal areas [6]. Satellite remote sensing technology is widely used to monitor and detect the dynamic changes in water quality parameters. This approach offers broad spatial and temporal coverage by utilizing various satellite sensors operating at visible and infrared wavelengths, enabling continuous and comprehensive observation of water conditions [7].

Sentinel-2A is capable of providing continuous and high-quality data that is highly supportive in providing water quality information through the Multi Spectral Imager (MSI) sensor. TSS can be estimated based on algorithms developed by Laili et al. [8], Budhiman [9], Liu et al. [10], and Parwati and Purwanto [11] from Sentinel-2A images. Therefore, the purpose of this study is to compare the accuracy of several algorithms using Sentinel-2A images with laboratory test results so that water quality evaluation can be identified quickly.

Although Sentinel-2 has been widely used for TSS estimation, the performance of empirical algorithms may vary among different water bodies because of differences in optical properties, suspended sediment characteristics, and local environmental conditions. Therefore, an algorithm developed and validated in one river, lake, or coastal environment may not provide similar accuracy when transferred to another region. In the downstream Krueng Aceh watershed, this issue is particularly relevant because the water environment is influenced by riverine processes, sediment transport, and anthropogenic activities. Therefore, this study compares four previously developed empirical TSS algorithms, namely Laili, Liu, Budhiman, and Parwati, using Sentinel-2 Level-2A imagery and laboratory-measured TSS data. The novelty of this study lies in evaluating the relative performance, regional suitability, and transferability of existing algorithms under the optical conditions of downstream Krueng Aceh, rather than developing a new TSS retrieval model. Accordingly, this study aims to identify which existing empirical algorithm provides the most suitable performance for TSS estimation in the study area.

2. MATERIAL AND METHODS

2.1 Study area

This research was conducted in the downstream area of the Krueng Aceh watershed (Figure 1). Primary data collection included Sentinel-2 Level-2A (surface reflectance) imagery acquired from the Copernicus Open Access Hub corresponding to the sampling date (26 August 2025), as well as surface water sampling at ten observation points distributed along the downstream Krueng Aceh. Surface water samples were collected on 26 August 2025 between 09:00 and 11:30 Western Indonesia Time (WIB), while the Sentinel-2C overpass occurred at 10:45 WIB, based on the metadata of product S2C_MSIL2A_20250826T034551_N0511_R104_T.

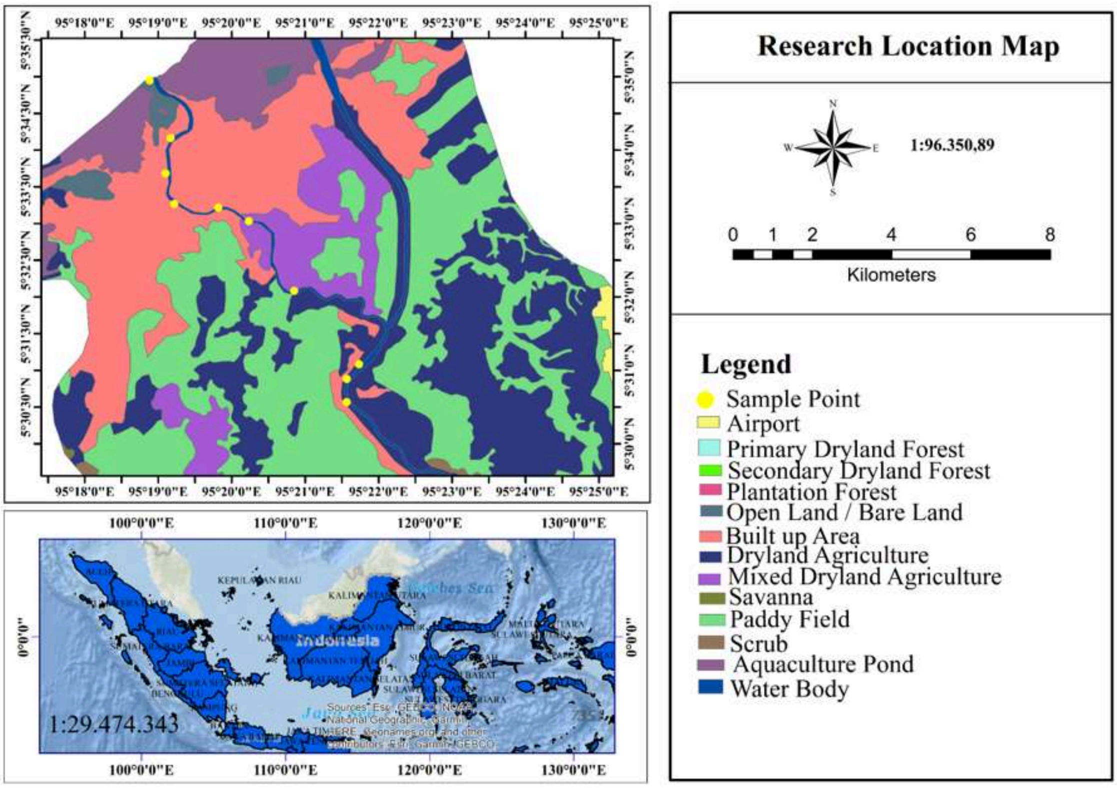

Figure 1. Area of study

The time difference between field sampling and satellite image acquisition ranged from 0 to 85 minutes, providing close temporal correspondence between the in-situ measurements and satellite observations. The ten sampling points were distributed to represent different levels of anthropogenic pressure, including urban activities, bridge and transportation areas, surface drainage, settlement areas, and shipping activities toward the river mouth. This spatial arrangement was intended to capture spatial variation in TSS associated with different human pressures along the downstream river system. Rainfall, river discharge, and tidal conditions were not directly measured during field sampling and are therefore recognized as factors that may influence the temporal representativeness of the dataset.

The water samples were analyzed in the laboratory to obtain TSS concentrations using the gravimetric method in accordance with SNI 6989.3:2019, providing in-situ data for validation.

The water samples were collected at a depth of 0–30 cm below the water surface and stored in 1-L plastic bottles. The samples were preserved in a cooler box at approximately 4 °C and transported to the Balai Standardisasi dan Pelayanan Jasa Industri (BSPJI) Banda Aceh, with a transport time of approximately 24 h before laboratory analysis. Before filtration, each sample was homogenized by stirring until uniform. A 10-mL aliquot was filtered under vacuum through a glass microfiber filter (Whatman GF/C or equivalent) with a nominal pore size of 1.2 µm. The filter was dried at 103–105 °C for 1–2 h until a constant weight was achieved, cooled to room temperature in a desiccator, and weighed using an analytical balance with a precision of 0.1 mg. A dried and pre-weighed blank filter was included in the analysis to account for filter mass. Each sample was analyzed in duplicate, and the TSS concentration reported in Table 1 represents the mean of the two analytical replicates. The gravimetric procedure followed SNI 6989.3:2019.

Table 1. Laboratory Total Suspended Solids (TSS) test results

No.	Location		Test TSS Laboratory (mg/L)
	Longitude	Latitude	
1	95°21'34" E	5°30'34" N	11.30
2	95°21'34" E	5°30'53" N	6.9
3	95°21'44" E	5°31'05" N	7.1
4	95°20'51" E	5°32'05" N	8.5
5	95°20'14" E	5°33'02" N	10.5
6	95°19'49" E	5°33'13" N	9.0
7	95°19'13" E	5°33'16" N	7.1
8	95°19'06" E	5°33'41" N	9.2
9	95°19'10" E	5°34'10" N	9.6
10	95°18'53" E	5°34'57" N	6.4

The Sentinel-2C Level-2A product (S2C_MSIL2A_20250826T034551_N0511_R104_T) was used directly as a Bottom-of-Atmosphere (BOA) surface-reflectance product that had already undergone atmospheric correction using the ESA Sen2Cor processor. Therefore, no additional atmospheric correction was applied. Image preprocessing was conducted using SNAP version 9.0. Cloud and cloud-shadow masking was performed using the Scene Classification Layer (SCL) and Band Math by excluding cloud-shadow (class 3), medium-probability cloud (class 8), high-probability cloud (class 9), and thin cirrus (class 10). The overall cloud coverage reported in the image metadata was 18.393832%. The GeoTIFF bands used in this study contained floating-point surface-reflectance values in the 0-1 range; therefore, no additional scaling factor, including division by 10,000, was applied. Water bodies were identified using the Normalized Difference Water Index (NDWI), with NDWI > 0 used as the threshold for water pixels. The bands were resampled to 10 m using the SNAP Resampling function (Raster → Geometric Operations → Resampling), and spectral reflectance values at each sampling location were extracted using a 3 × 3 pixel window with mean aggregation.

Field sampling and Sentinel-2 image acquisition were conducted on the same date (26 August 2025) to ensure temporal consistency between in-situ and satellite observations. TSS was analyzed gravimetrically following SNI 6989.3:2019. Water pixels were extracted using NDWI with a threshold of NDWI > 0. The four empirical TSS algorithms were applied at the pixel level for each sampling location.

To generate the spatial distribution map of laboratory-measured TSS, the ten sampling points were interpolated using the Ordinary Kriging method in ArcGIS. Ordinary Kriging estimates TSS values at unsampled locations based on the spatial relationship among the observed sampling points, thereby producing a continuous predicted TSS surface from the ten laboratory observations. The interpolated TSS surface was generated at a 10-m spatial resolution and projected using WGS 84 / UTM Zone 47 N. The interpolation result was clipped using the water mask derived from the NDWI threshold (NDWI > 0), while areas outside the water mask were treated as no-data and excluded from the TSS distribution map. For visualization, the predicted TSS values were divided into five classes using the Equal Interval classification method in ArcGIS. The class boundaries were determined from the minimum and maximum predicted TSS values generated by the interpolation process. Therefore, the laboratory-based TSS map represents a spatially interpolated prediction surface rather than direct measurements at every raster cell.

2.2 Data and methodology

In this research, data analysis focused on estimating TSS concentrations using Sentinel-2 Level-2A imagery through the application of four empirical algorithms that have been tested in hydro-optical studies of water bodies. The selection of multiple algorithms was carried out to test the accuracy and suitability of the model with the bio-optical characteristics of the waters in the Krueng Aceh Hilir watershed. The four algorithms used are mentioned below:

The first algorithm [8] was developed for Poteran Waters, East Java.

$$\text{TSS} = 31.42\,\frac{Log\ (Band\ 2)}{Log\ (Band\ 4)} - 12.719$$

The second algorithm [9] was developed for the Mahakam River, East Borneo.

$$\text{TSS} = 8.1429 \times exp(23.704 \times 0.94 \times Band\ 4)$$

The third algorithm [10] was developed for Poyang Lake, China.

$$\text{TSS} = 2.950\ (Band\ 7^{1.357})$$

The fourth algorithm [11] was developed for Berau Waters, Indonesia.

$$TSS = 3.3238 \times exp(34.099 \times Band\ 4)$$

The four published empirical algorithms were originally developed for different sensors and aquatic environments. Therefore, their application to Sentinel-2 requires consideration of spectral-band correspondence and reflectance scaling. In this study, all four algorithms were applied directly to Sentinel-2 Level-2A surface-reflectance data without local recalibration. The Sentinel-2 bands were selected based on their spectral correspondence with the bands specified in the original empirical formulations. The original equation forms and coefficients were retained without modification. This approach was used to evaluate the direct transferability of the published algorithms to the optical conditions of the downstream Krueng Aceh watershed.

The published empirical algorithms (Laili, Liu, Budhiman, and Parwati) were applied using their original coefficients without recalibration or refitting. The relationship between laboratory-measured TSS concentrations and algorithm-derived TSS estimates was evaluated using regression analysis. Therefore, leave-one-out cross-validation (LOOCV) was not used to modify the published algorithm formulations or to estimate new algorithm coefficients. Instead, LOOCV was used as a performance-stability assessment under the small-sample condition of this study. At each iteration, nine observations were used to fit the linear relationship between the laboratory-measured TSS and the TSS estimates produced by a given published algorithm, while the remaining observation was retained for validation. This procedure was repeated ten times so that each observation served once as the validation observation. The final RMSE, MAPE, and R^2 values were calculated from the aggregated LOOCV predictions. Accordingly, the LOOCV results are interpreted as an assessment of the stability of the observed algorithm–field-data relationship under limited sample size rather than as a direct measure of the intrinsic generalization capability of the published fixed-coefficient algorithms.

$$Y = a + bX$$

where,

Y = Dependent variable or concentration value of TSS Laboratory (mg/L)

X = Independent variable (Sentinel Image)

a = Constant (intercept)

b = Regression coefficient (slope)

RMSE measures the average absolute error between the actual value and the predicted value. The lower the RMSE value, the more accurate the model to predict the TSS value.

$$\text{MAPE} = \frac{1}{N}\sum_{t=1}^{n}\left|\frac{Y_t - \hat{Y}_t}{Y_t}\right| \times 100\%$$

where,

Y_t = Actual Value

$\hat{Y}_t$ = Prediction Value

N = Numbers of Data In predicting the turbidity

The coefficient of determination (R^2) is used to evaluate the proportion of variation in the observed TSS values that is explained by the predicted TSS values. The R^2 value ranges from 0 to 1, with values closer to 1 indicating a stronger agreement between predicted and observed TSS values, whereas values closer to 0 indicate a weaker explanatory relationship. R^2 was calculated using the following equation:

$$R^2 = 1 - (1 + x)^n = 1\frac{\sum_t^N = 1\,(T - \hat{T})^2}{\sum_t^N = 1(T - \check{T})^2}$$

where,

N = Number of data

T = Actual TSS value

$\hat{T}$ = Predicted TSS value

$\check{T}$ = Actual average TSS value

3. RESULTS

One of the limitations in the application of remote sensing lies in the variation in spatial, temporal, and spectral resolution of the sensors used in the data acquisition process. Sensors with long re-recording intervals tend to have limitations in detecting the temporal dynamics of water quality parameters, such as TDS and TSS. Each satellite sensor has different resolution characteristics in terms of spatial, spectral, and temporal aspects. For example, Landsat 8 OLI has a revisit period of approximately 16 days, while Sentinel-2A/B MSI offers a shorter interval of approximately 5 days, making it more optimal for detecting temporal changes in water quality [12, 13].

The results of TSS measurements through laboratory tests from 10 sampling points in the Krueng Aceh Hilir watershed are presented in Table 1. Samples were taken at geographically dispersed locations with longitude coordinates varying from 95°18'53" E to 95°21'44" E and latitude coordinates varying from 5°30'34" N to 5°34'57" N. The laboratory test data showed variations in TSS values among the ten sampling points and were used as observed TSS values for evaluating the performance of the empirical algorithms. Because no independent test dataset was available, model performance was assessed using LOOCV.

The ten sampling points represented different downstream settings with varying levels of anthropogenic activity. Points 1-4 were located in the Lambaro area, which includes market activities, water-treatment infrastructure, agricultural areas, livestock activities, and river infrastructure. Points 5-9 were located in the urban area of Banda Aceh, characterized by dense settlements, bridges, commercial activities, and boat-mooring areas. Point 10 was located near the river mouth, close to the coastal zone.

The highest laboratory-measured TSS concentration was observed at Point 1 (11.3 mg/L), followed by Point 5 (10.5 mg/L), Point 9 (9.6 mg/L), and Point 8 (9.2 mg/L). The relatively high TSS concentration at Point 1 may be associated with intensive activities around Lambaro Market, although this relationship was not directly tested because land-use intensity, rainfall, and runoff were not measured. The TSS concentration at Point 2 was lower (6.9 mg/L), which may reflect differences in local environmental conditions and anthropogenic activities around the water-treatment facility. Point 3 recorded 7.1 mg/L, while Point 4 recorded 8.5 mg/L; the observed variation may be related to local flow conditions, sedimentation, and surrounding agricultural and livestock activities. However, these factors were not directly measured in this study and therefore cannot be confirmed as causes of the observed TSS differences.

Points 5-9 showed spatial variability in TSS concentrations within the urban downstream section. Point 5 recorded 10.5 mg/L, which may be associated with the surrounding dense settlement and urban drainage network. Point 6 recorded 9.0 mg/L, whereas Point 7 recorded 7.1 mg/L, indicating local differences in TSS conditions despite their urban setting. Point 8 recorded 9.2 mg/L and was located in an area with dense settlements and commercial activities. Point 9 recorded 9.6 mg/L near the boat-mooring area in Kampung Jawa. Vessel activity and sediment disturbance may be possible explanations for the relatively high TSS value at this location; however, vessel traffic was not measured during sampling.

The lowest TSS concentration was observed at Point 10 (6.4 mg/L), located near the river mouth. This relatively low value may be associated with mixing between river and seawater and tidal dynamics; however, tidal conditions, river discharge, and rainfall were not measured during the survey. Therefore, these factors should be considered possible explanations rather than demonstrated causes.

Estimation of TSS concentrations obtained from Sentinel-2 Level-2A image processing using four estimation algorithms, namely Laili et al. [8], Budhiman [9], Liu et al. [10], and Parwati and Purwanto [11], at each sampling location is presented in Table 2. The results illustrate spatial variation in TSS estimates and differences among the four algorithms at the same sampling locations. These values were compared with laboratory measurements to evaluate the performance of each image-based estimation method.

The estimation of TSS values using Sentinel-2 Level 2A imagery produced significant variations in values between the four algorithms applied (Figure 2). A comparative analysis reveals quite striking estimation disparities, with the Liu algorithm showing a tendency for high estimates at certain locations, particularly sampling location points 4 and 5, which reached 86.33 mg/L and 64.68 mg/L. These high values indicate that the Liu algorithm is highly sensitive to changes in reflectance in the red and near-infrared bands used in its calculations, enabling it to detect significant increases in suspended material in more turbid waters. On the other hand, lower values such as at location 6 (8.39 mg/L), location 8 (8.30 mg/L), and location 9 (10.33 mg/L) demonstrate the algorithm's ability to capture spatial variations between high and low TSS areas. The average TSS value in Liu's algorithm was at a medium to high level, indicating that this model tends to overestimate areas with high reflectance due to the presence of suspended materials and other optical elements such as phytoplankton or organic matter.

Table 2. Total Suspended Solids (TSS) measurement data from Sentinel-2 Level-2A

No.	Location		Predicted TSS Method (mg/L)			
	Longitude	Latitude	Liu	Laili	Budhiman	Parwati
1	95°21'34" E	5°30'34" N	155.63	19.79	23.12	23.37
2	95°21'34" E	5°30'53" N	26.69	18.14	28.48	22.58
3	95°21'44" E	5°31'05" N	16.81	17.94	27.73	21.68
4	95°20'51" E	5°32'05" N	86.33	17.50	17.36	10.59
5	95°20'14" E	5°33'02" N	64.68	19.21	40.86	39.24
6	95°19'49" E	5°33'13" N	8.39	18.44	11.99	6.01
7	95°19'13" E	5°33'16" N	10.23	17.99	11.68	5.77
8	95°19'06" E	5°33'41" N	8.30	18.23	12.65	6.52
9	95°19'10" E	5°34'10" N	10.33	19.41	12.37	6.31
10	95°18'53" E	5°34'57" N	18.17	15.03	12.29	6.24

The Laili's algorithm shows relatively stable TSS estimates, with values ranging from 15.03 to 19.79 mg/L. The highest recorded value was at location 1, with 19.79 mg/L, while the lowest value was at location 10, with 15.03 mg/L. The values at the other locations also showed relatively small variations, indicating the stability of the model in estimating TSS concentration. The consistency of these values indicates that Laili's algorithm has moderate sensitivity to changes in water spectral characteristics, which is likely due to the use of interband ratios in the model formulation, thereby reducing the influence of reflectance anomalies and non-sediment materials.

The Budhiman's algorithm estimates TSS concentrations ranging from 11.68 to 40.86 mg/L, with the maximum value observed at location 5 (40.86 mg/L) and the minimum value at location 7 (11.68 mg/L). Location 2 (28.48 mg/L) and location 3 (27.73 mg/L) also showed relatively high TSS values, indicating higher concentrations of suspended solids at these sampling locations. Parwati's algorithm produced TSS estimates ranging from 5.77 to 39.24 mg/L, with the highest value recorded at location 5 (39.24 mg/L) and the lowest value at location 7 (5.77 mg/L). At several locations, particularly location 6 (6.01 mg/L), location 7 (5.77 mg/L), location 8 (6.52 mg/L), and location 9 (6.31 mg/L), the estimates showed relatively low values with narrow variability, indicating the stability of the algorithm's estimates under low TSS conditions.

To assess the stability of the observed relationships between laboratory-measured TSS and the estimates generated by the four published algorithms under the limited sample size, the non-cross-validated results were compared with the LOOCV results (Table 3). Because the algorithms were applied using their original fixed coefficients, LOOCV was used as a performance-stability assessment rather than as a recalibration procedure.

Table 3. Comparison of non-cross-validated and leave-one-out cross-validation (LOOCV) performance of the four empirical Total Suspended Solids (TSS) algorithms

Algorithm	Metric	No CV	LOOCV
Liu	RMSE (mg/L)	1.2377	1.4788
Liu	MAPE (%)	14.4032	17.4274
Liu	R^2	0.3784	0.1126
Laili	RMSE (mg/L)	0.9799	1.5163
Laili	MAPE (%)	10.9420	16.1822
Laili	R^2	0.6103	0.0670
Budhiman	RMSE (mg/L)	1.5215	1.9466
Budhiman	MAPE (%)	16.5546	21.0847
Budhiman	R^2	0.0607	-0.5376
Parwati	RMSE (mg/L)	1.4619	1.7957
Parwati	MAPE (%)	16.1826	20.0446
Parwati	R^2	0.1328	-0.3084

Note: CV: cross-validation.

The results show a substantial difference between the non-cross-validated and LOOCV performance. Under LOOCV, the Laili algorithm produced the lowest RMSE (1.5163 mg/L) and MAPE (16.1822%) among the four algorithms, whereas the Liu algorithm produced the highest R^2 (0.1126). However, the R^2 value for Laili was only 0.0670, indicating limited predictive ability for the available observations. Liu also showed a low R^2 of 0.1126, while Budhiman and Parwati produced negative R^2 values of -0.5376 and -0.3084, respectively. Thus, although Laili showed the best relative performance among the four algorithms under LOOCV, its predictive ability remained weak.

The non-cross-validated results showed apparently better performance, particularly for Laili, with RMSE = 0.9799 mg/L, MAPE = 10.9420%, and R^2 = 0.6103. These statistics were calculated from the complete set of observations and may therefore provide an optimistic representation of the observed algorithm–field-data relationship under the small-sample condition. In contrast, the lower LOOCV performance indicates that this relationship was not stable when individual observations were sequentially excluded from the regression assessment. Therefore, the LOOCV results are considered the primary indicators for assessing performance stability in this study. The findings should be regarded as preliminary, and larger multi-season datasets with independent validation are required for a more robust assessment of the four published algorithms.

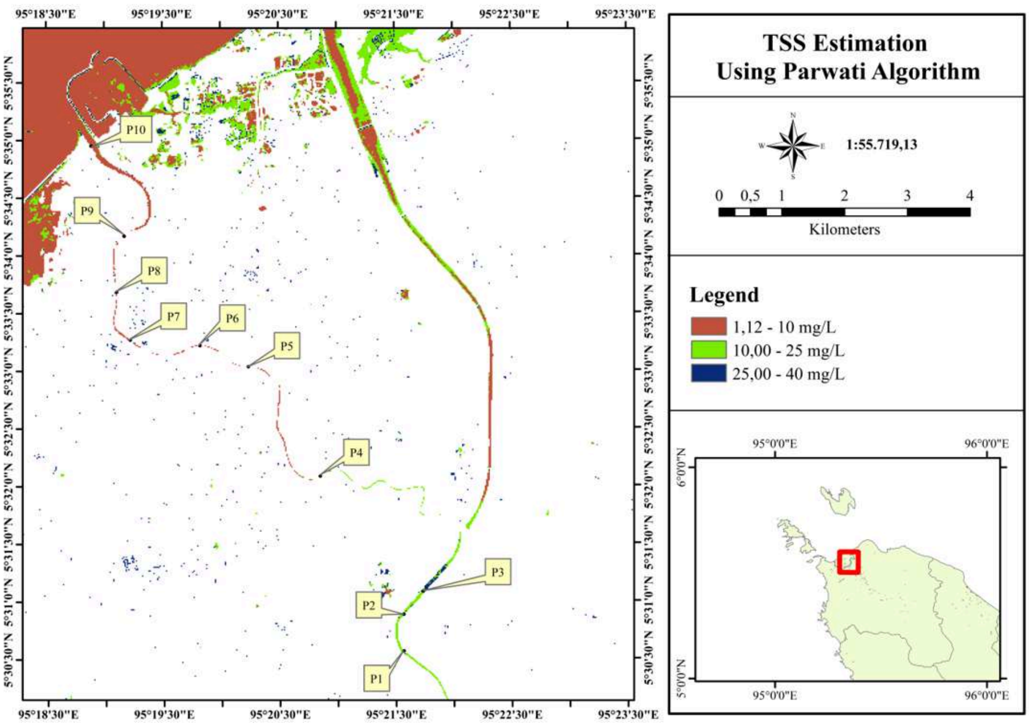

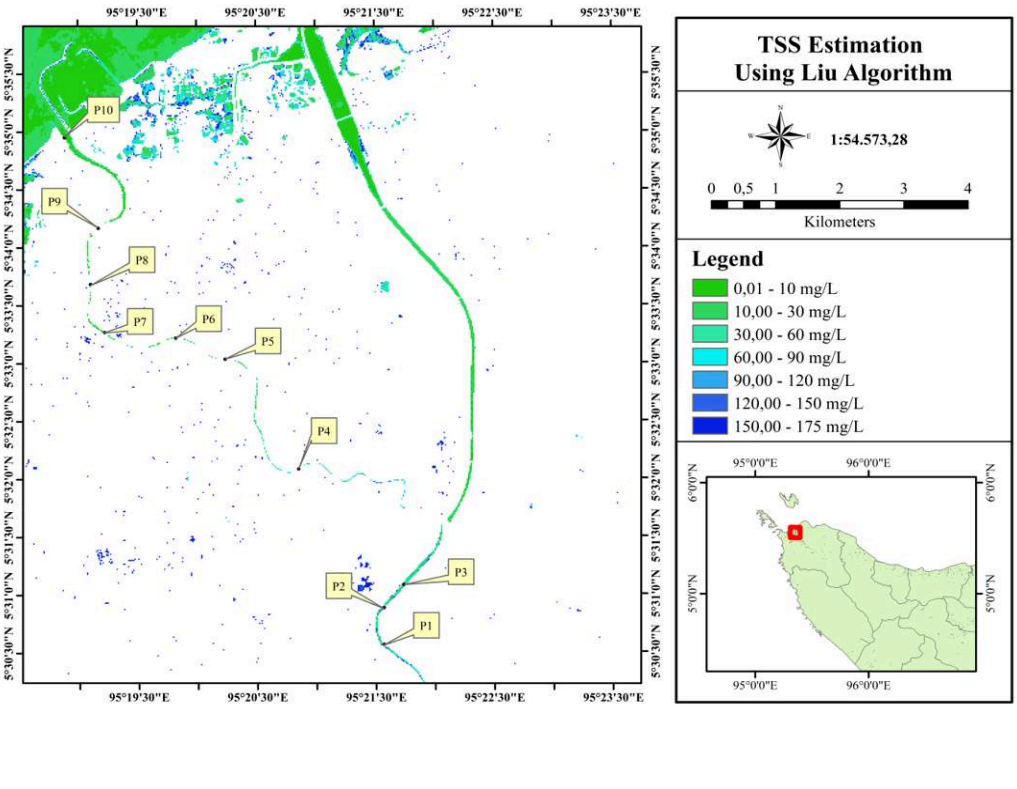

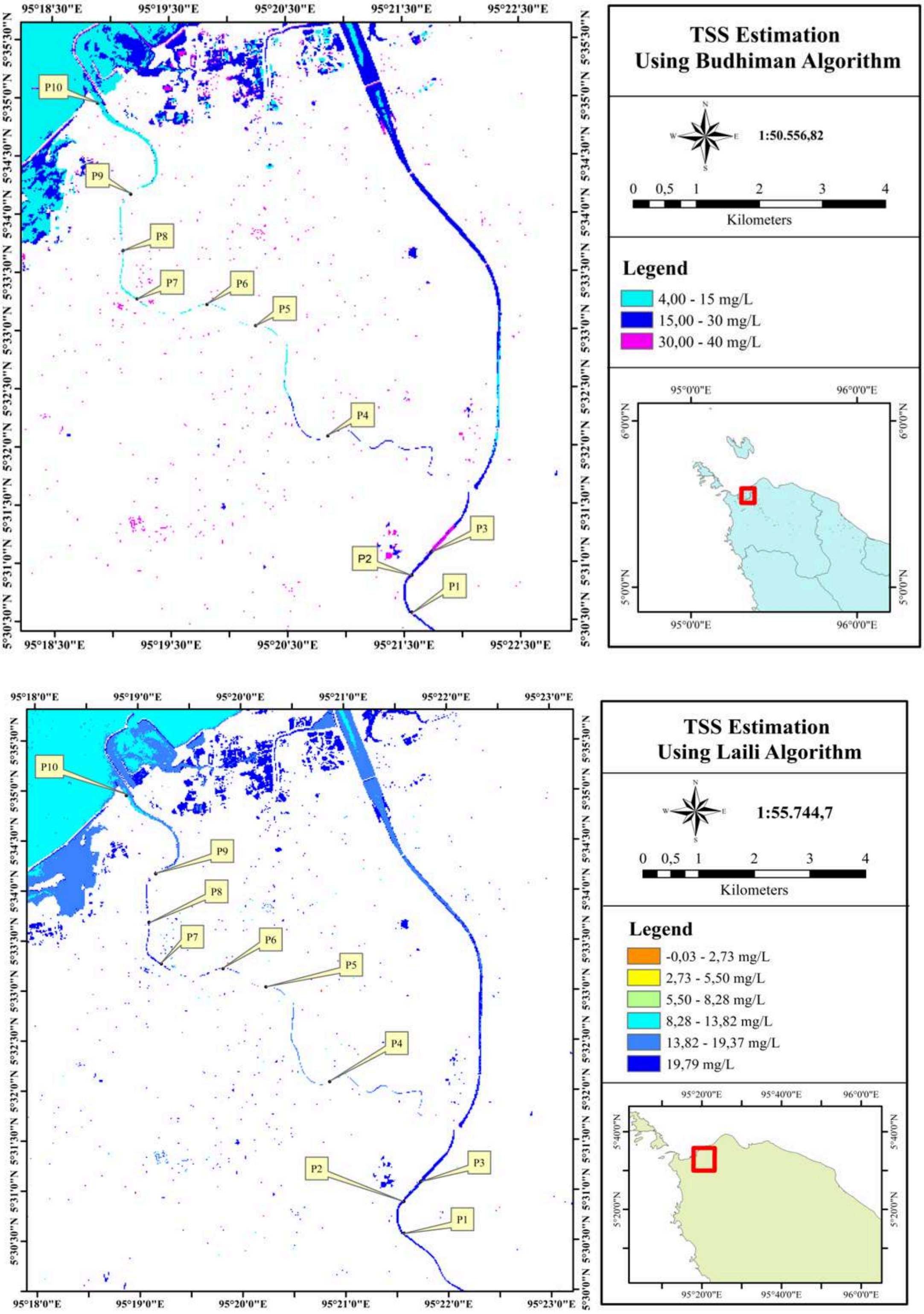

Figure 2. Total Suspended Solids (TSS) estimation results using several different algorithms

The comparison between in-situ measurements and the estimation results using satellite imagery was tested using a regression model. The relationship between parameter values can be seen in Figure 3.

The non-cross-validated (No CV) regression statistics are presented in Table 4 to provide a descriptive comparison of the relationships between laboratory-measured TSS and the estimates generated by the four algorithms. Laili showed the lowest non-cross-validated RMSE (0.9799 mg/L), MAE (0.8661 mg/L), and MAPE (10.94%), with an R^2 of 0.6103. However, these statistics should be interpreted only as descriptive, non-cross-validated results because they do not account for the stability of the regression relationship under the limited sample size. The corresponding LOOCV results provide a more conservative assessment and indicate substantially lower predictive performance, particularly for Laili (R^2 = 0.0670). Therefore, the non-cross-validated statistics are not used as the primary basis for ranking the algorithms.

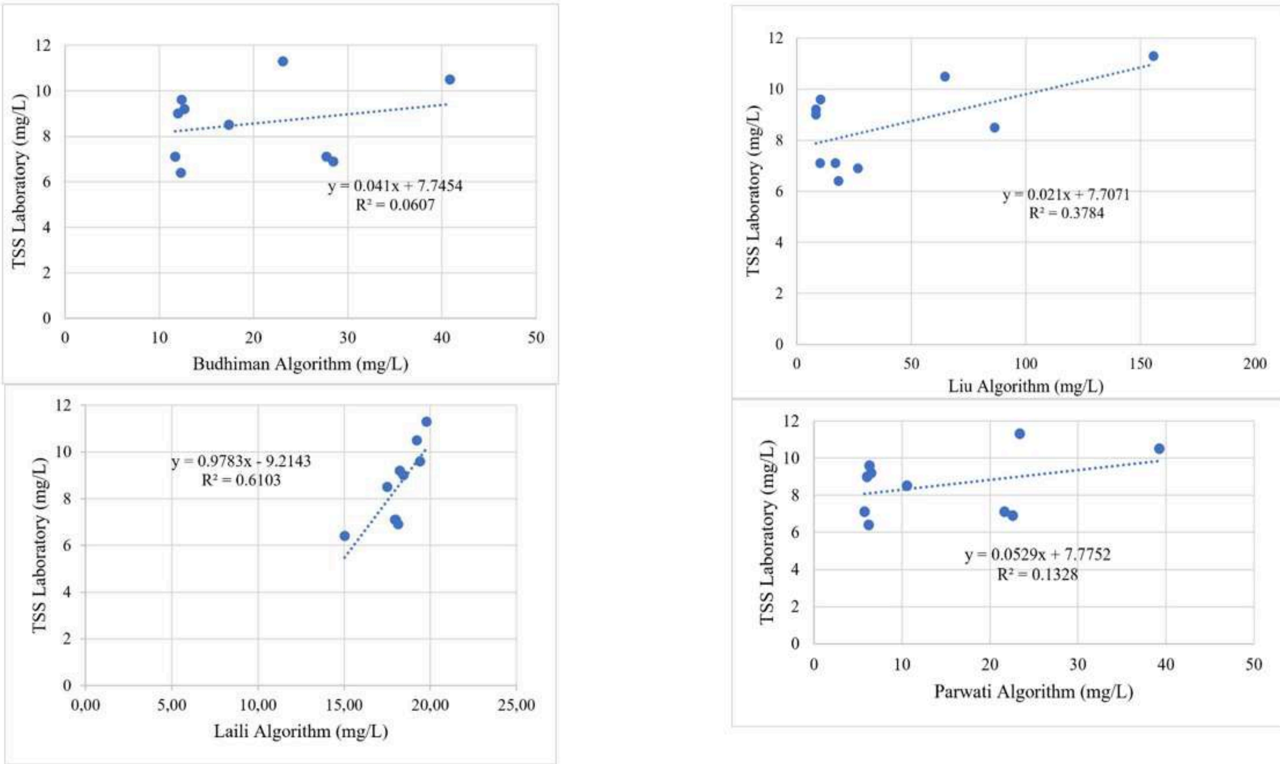

Figure 3. Linear regression analysis results for the algorithm

Table 4. Non-cross-validated (No CV) regression statistics of the four empirical Total Suspended Solids (TSS) algorithms

Algorithm	RMSE	MAE	BIAS	MAPE (%)	Slope	Intercept	R^2
Liu	1.23766	1.0016	-0.1068	14.40	0.0210	7.7071	0.3784
Laili	0.9799	0.8661	-0.0005	10.94	0.9783	-9.2143	0.6103
Budhiman	1.5229	1.2443	0.2929	16.56	0.0410	7.7454	0.0607
Parwati	1.4618	1.2025	0.0304	16.18	0.0529	7.7752	0.1328

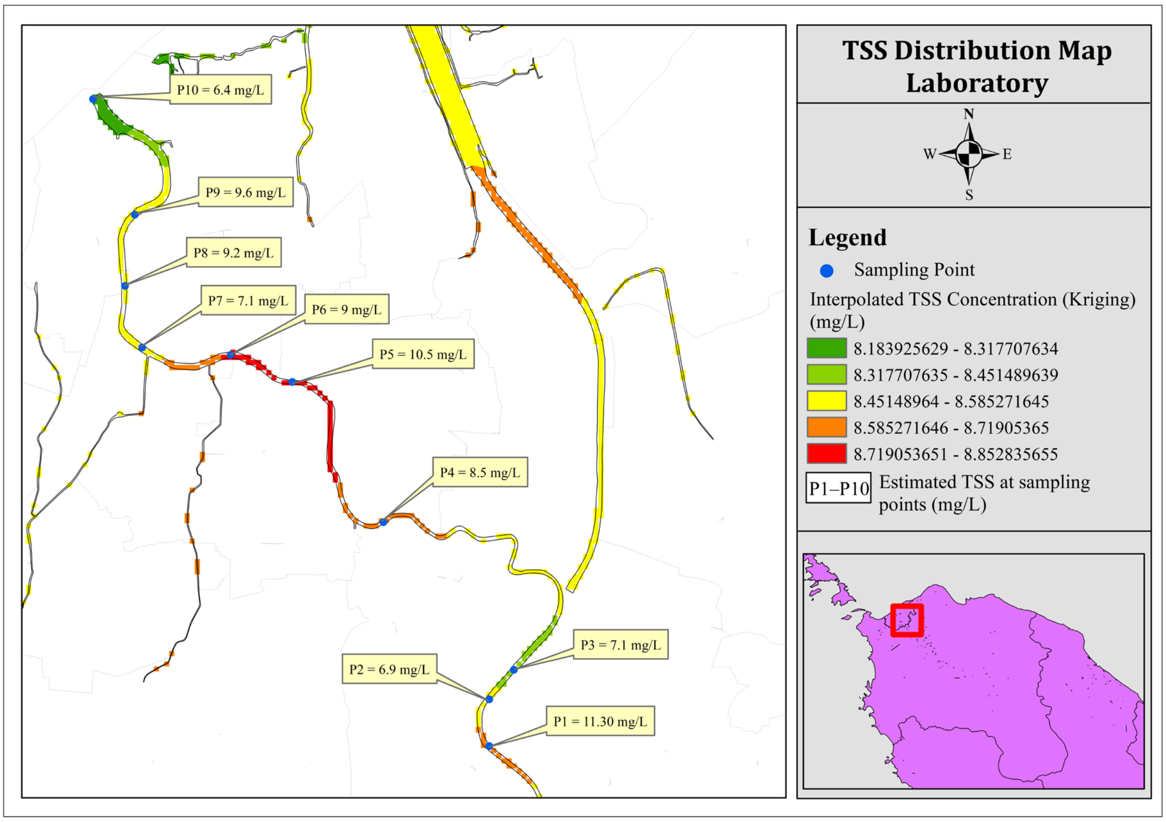

Figure 4. Ordinary Kriging-based interpolated spatial distribution of laboratory-measured Total Suspended Solids (TSS) and observed sampling points in the downstream Krueng Aceh watershed

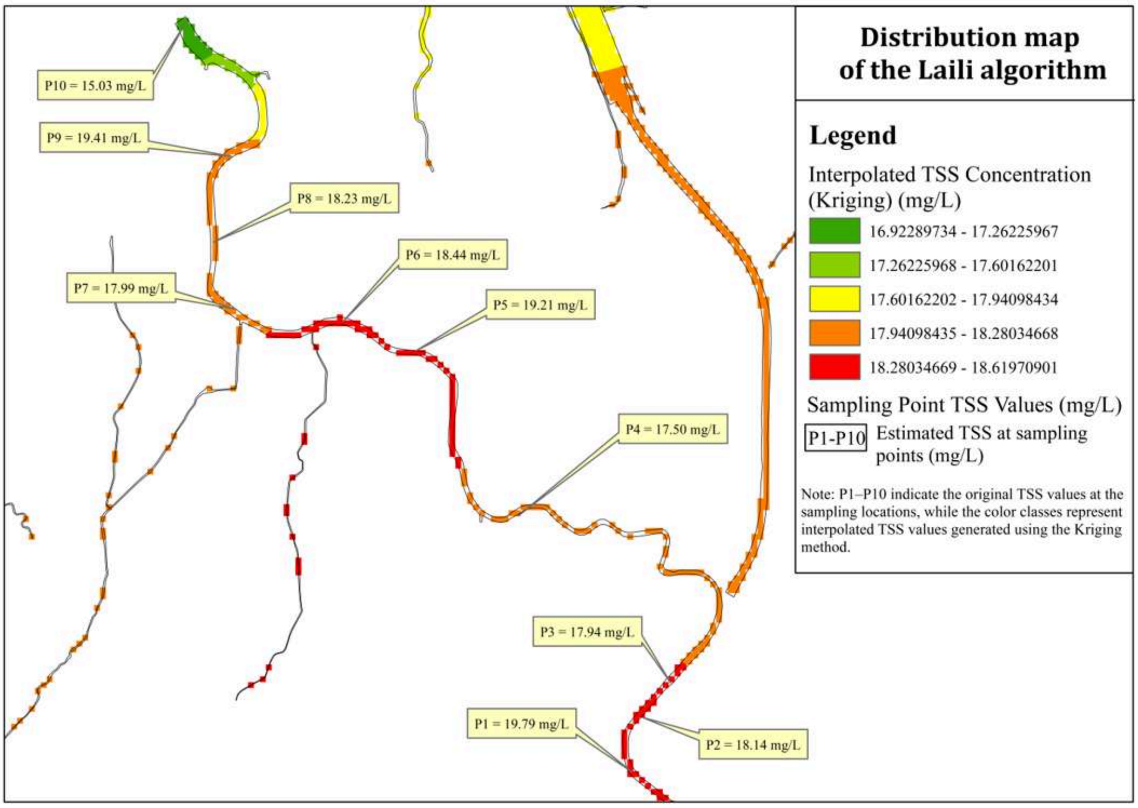

Figure 5. Spatial distribution of Total Suspended Solids (TSS) estimated using the Laili et al. [8] algorithm in the downstream Krueng Aceh watershed

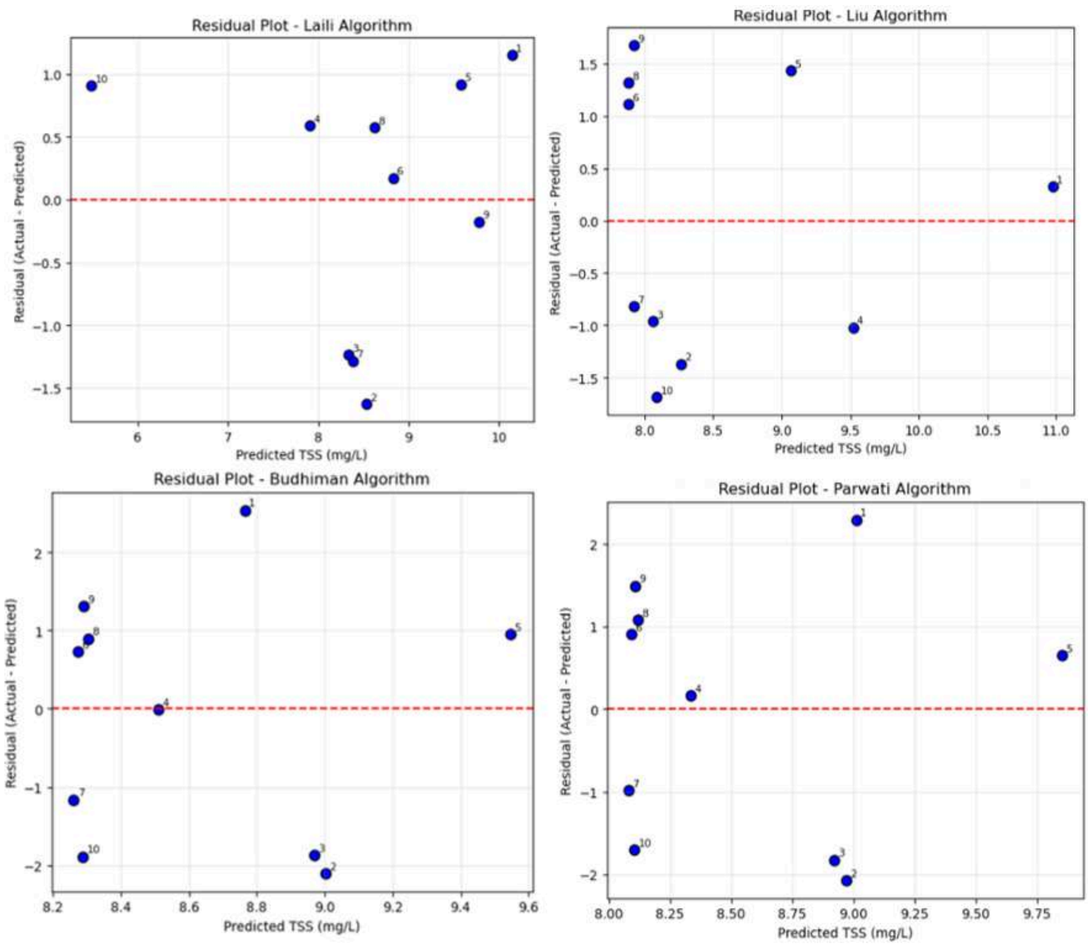

Figure 6. Residual plots based on regression-predicted Total Suspended Solids (TSS) values for the four empirical algorithms

The spatial distribution of laboratory-measured TSS was generated by interpolating the ten sampling points using Ordinary Kriging. The resulting map represents a continuous predicted TSS surface between the observed sampling locations rather than direct laboratory measurements at every raster cell. The values shown in the map legend represent the interpolated TSS values generated by the Ordinary Kriging process, whereas the observed TSS values measured at the ten sampling points ranged from 6.4 to 11.30 mg/L, as reported in Table 1. The sampling points shown on the map indicate the locations of the field observations used as input data for the interpolation. The predicted values were mapped at a 10-m spatial resolution within the water mask and classified into five equal-interval classes, as shown in Figure 4.

The spatial distribution of TSS estimated using the Laili et al. [8] algorithm is presented in Figure 5. Based on the results in Table 2, the estimated TSS values at the ten sampling points ranged from 15.03 to 19.79 mg/L. The highest estimated value was recorded at Sampling Point 1 (19.79 mg/L), whereas the lowest value was recorded at Sampling Point 10 (15.03 mg/L). The values estimated at the ten sampling points were used to represent the spatial distribution of TSS across the downstream Krueng Aceh watershed. Figure 5 shows the spatial pattern of the estimated TSS values, classified into five equal-interval classes to facilitate visualization of their spatial variation.

Residual analysis was further conducted to examine the distribution and systematic patterns of prediction errors for each empirical algorithm. The residual plots are presented in Figure 6. The predicted TSS values shown on the x-axis were obtained from the linear regression fitting between the laboratory-measured TSS values and the TSS values estimated using each published empirical algorithm. Thus, the predicted TSS values in Figure 6 represent regression-fitted values rather than the original algorithm-derived TSS values reported in Table 2. The residuals were calculated as the differences between the laboratory-measured TSS values and the regression-predicted TSS values. These plots provide additional information on the magnitude, direction, and potential systematic structure of prediction errors that cannot be fully captured by RMSE, MAPE, and R^2 alone.

4. DISCUSSION

TSS is an important indicator in assessing water quality because it affects turbidity and transparency levels, which directly impact the photosynthesis process of aquatic organisms and ecosystem balance. High TSS levels can reduce water quality, decrease dissolved oxygen levels, and disrupt the habitats of species living in the water [14].

TSS is closely related to soil erosion and river channel erosion. TSS levels vary, ranging from less than 5 mg/L to as high as 30.000 mg/L in some rivers. TSS is not only an important measurement for erosion levels in river channels, but is also related to the transport of nutrients (especially phosphorus), metals, and various industrial and agricultural chemicals through river systems. The spatial distribution of TSS should be thoroughly understood. Sediment is commonly found at the foot of mountains, along waterways and rivers, and within reservoirs. Sedimentation is the process of depositing materials into water bodies as a result of erosion. This process involves the accumulation of soil particles influenced by water flow velocity, allowing the sediment to reach its settling velocity. Prolonged periods of intense rainfall can exacerbate this condition by increasing sediment accumulation in river channels, thereby reducing their water storage capacity and posing significant hazards [15].

The TSS value and turbidity level are positively correlated; this means that the higher the TSS value, the higher the turbidity value [16]. High water turbidity restricts light penetration into the water column, thereby affecting the metabolism of aquatic organisms [17]. An increase in the concentration of suspended solids causes turbidity, which inhibits the penetration of sunlight into the water. As a result, the low light intensity inhibits the growth of phytoplankton [18].

The non-cross-validated results showed that the Laili algorithm had the strongest observed relationship with the laboratory-measured TSS, with RMSE = 0.9799 mg/L, MAPE = 10.9420%, and R^2 = 0.6103. However, the LOOCV results showed a substantial reduction in performance, with RMSE = 1.5163 mg/L, MAPE = 16.1822%, and R^2 = 0.0670. This difference indicates that the apparent relationship observed in the complete dataset was not stable under the limited sample size. Among the four algorithms, Laili still produced the lowest LOOCV RMSE and MAPE, although its low R^2 indicates weak predictive ability. Therefore, the results should be interpreted as a comparative assessment of performance stability rather than as evidence of strong predictive capability.

The differences in algorithm performance may reflect the sensitivity of the empirical formulations to the optical and environmental characteristics of the study area. Each algorithm was developed under specific environmental, optical, and regional conditions, and differences in water composition, sediment characteristics, and spectral response may affect its performance when applied to another river system. In this study, the original coefficients of all four published algorithms were retained without recalibration or refitting. Therefore, the differences observed among the algorithms represent their relative performance under the specific conditions of the downstream Krueng Aceh watershed rather than the performance of newly optimized models. The relatively low LOOCV performance also indicates that the relationship between the field measurements and algorithm-derived estimates was sensitive to the limited number of observations.

Previous research has also demonstrated the potential of remote sensing for monitoring suspended sediment and water quality. Ramli et al. [19] applied the Modified Universal Soil Loss Equation (MUSLE) to estimate annual erosion and used a log-ratio-based algorithm with Landsat-8 imagery to map the spatial distribution of TSS. The study demonstrates the potential of integrating erosion modelling and satellite-based observations to investigate sediment dynamics. However, remote-sensing-based TSS estimation can be affected by spatial resolution, spectral characteristics, atmospheric conditions, and the complexity of water environments. These limitations may become more pronounced in narrow river channels and areas with complex shoreline morphology, where mixed pixels and high spatial variability can influence the extracted spectral information.

Research conducted by Sent et al. [20] also demonstrated the potential of the Sentinel-2 MSI for monitoring water-quality parameters, particularly turbidity. The ability of Sentinel-2 to provide multispectral observations at relatively fine spatial resolution allows spatial variations in suspended particles and related water-quality conditions to be assessed over broader areas than conventional field measurements. However, the accuracy of satellite-derived water-quality estimates remains dependent on the relationship between spectral reflectance and in-situ measurements, as well as on environmental and hydrological conditions at the time of image acquisition. Therefore, satellite observations are most effectively used in combination with field measurements to evaluate the applicability of empirical algorithms under specific local conditions.

Finally, the present findings are based on a single Sentinel-2 acquisition and one field-sampling campaign conducted on 26 August 2025. Therefore, the results represent the conditions observed during the study period and cannot be assumed to represent wet-season, dry-season, or flood-event conditions. In addition, the limited number of field observations restricts the strength of the performance assessment. Multi-season observations, a larger number of field samples, and independent validation under different hydrological conditions are required to determine the robustness and broader applicability of the evaluated algorithms.

5. CONCLUSION

This study compared four published empirical algorithms, namely Laili, Liu, Budhiman, and Parwati, for TSS estimation using Sentinel-2C Level-2A imagery and field measurements in the downstream Krueng Aceh watershed. All algorithms were applied using their original fixed coefficients without recalibration or refitting. The non-cross-validated results showed that Laili produced the strongest observed relationship with laboratory-measured TSS (RMSE = 0.9799 mg/L, MAPE = 10.9420%, and R^2 = 0.6103). However, its LOOCV performance decreased to RMSE = 1.5163 mg/L, MAPE = 16.1822%, and R^2 = 0.0670, indicating limited stability under the small-sample condition.

Among the four algorithms, Laili showed the best relative performance under LOOCV based on the lowest RMSE and MAPE. However, its low R^2 indicates limited predictive ability, while the negative R^2 values obtained for Budhiman and Parwati indicate poor stability of their relationships with the field observations. Therefore, the results represent a comparative assessment of the performance stability of the published algorithms under the specific conditions of the study area rather than evidence of a universally superior algorithm.

The study demonstrates the potential of Sentinel-2 imagery for spatial assessment of TSS in the downstream Krueng Aceh watershed. However, the findings are limited to a single Sentinel-2 acquisition, one field-sampling campaign, and ten observations. Larger multi-season datasets, additional field measurements, and independent validation under different hydrological conditions are recommended to establish the robustness and broader applicability of the evaluated algorithms.

ACKNOWLEDGMENT

This research was supported by Universitas Syiah Kuala through the Professor Research Grant funded by the Ministry of Higher Education, Science, and Technology of the Republic of Indonesia, under the Research Implementation Assignment Agreement for Fiscal Year 2025, Contract No. 298/UN11.1.1/PG.01.03/14652-PTNBH/2025, dated 15 July 2025.

REFERENCES

[1] Ellis, E.A., Allen, G.H., Riggs, R.M., Gao, H.L., Li, Y., Carey, C.C. (2024). Bridging the divide between inland water quantity and quality with satellite remote sensing: An interdisciplinary review. Wiley Interdisciplinary Reviews: Water, 11(4): e1725. https://doi.org/10.1002/wat2.1725

[2] Al Hakim, M.A.G., Susilo, S.B., Gaol, J.L. (2023). Turbidity front detection using Sentinel-2 satellite image relationship with oceanography in Bengawan Solo estuary. Jurnal Ilmu dan Teknologi Kelautan Tropis, 14(3): 337-352. https://doi.org/10.29244/jitkt.v14i3.40172

[3] Nurmalita, M., Maulidia, Syukri, M. (2013). Analysis of turbidity and sediment content and their relationship with the watershed condition of the Krueng Aceh River. In Proceedings of the National Seminar on Community-Based Watershed Management Towards Sustainable Aceh Forests. https://www.researchgate.net/profile/Nurmalita-Nurmalita/publication/344016416_Seminar_Nasional/links/5f4e331592851c6cfd1e2a4a/Seminar-Nasional.pdf.

[4] Junaidi, T.J., Ramli, I., Aliasuddin. (2025). Analysis of environmental carrying capacity based on water supply ecosystem services in the Seulawah Valley sub-district. IOP Conference Series: Earth and Environmental Science, 1477(1): 012018. https://doi.org/10.1088/1755-1315/1477/1/012018

[5] Jonianto, J., Ramli, I., Suhendrayatna, S., Mulyati, S., Mariana, M. (2026). Assessment of leachate treatment efficiency and its impact on surface water quality at the Blang Bintang Landfill, Aceh Besar. Jurnal Teknik Pertanian Lampung (Journal of Agricultural Engineering), 15(3): 1115-1129. https://doi.org/10.23960/jtepl.v15i3.1115-1129

[6] Sòria-Perpinyà, X., Vicente, E., Urrego, P., et al. (2021). Validation of water quality monitoring algorithms for Sentinel-2 and Sentinel-3 in Mediterranean inland waters with in situ reflectance data. Water, 13(5): 686. https://doi.org/10.3390/w13050686

[7] Amani, M., Ghorbanian, A., Ahmadi, S.A., et al. (2020). Google Earth Engine cloud computing platform for remote sensing big data applications: A comprehensive review. IEEE Journal of Selected Topics in Applied Earth Observations and Remote Sensing, 13: 5326-5350. https://doi.org/10.1109/JSTARS.2020.3021052

[8] Laili, N., Arafah, F., Jaelani, L.M., et al. (2015). Development of water quality parameter retrieval algorithms for estimating total suspended solids and chlorophyll-a concentration using Landsat-8 imagery at Poteran Island water. ISPRS Annals of the Photogrammetry, Remote Sensing and Spatial Information Sciences, 2(2W2): 55-62. https://doi.org/10.5194/isprsannals-II-2-W2-55-2015

[9] Budhiman, S. (2004). Mapping TSM concentrations from multi sensor satellite images in turbid tropical coastal waters of Mahakam Delta Indonesia. MSc Thesis, ITC Enschede, The Netherlands.

[10] Liu, H.Z., Li, Q.Q., Shi, T.Z., Hu, S.B., Wu, G.F., Zhou, Q.M. (2017). Application of Sentinel 2 MSI images to

retrieve suspended particulate matter concentrations in Poyang Lake. Remote Sensing, 9(7): 761. https://doi.org/10.3390/rs9070761

[11] Parwati, E., Purwanto, A.D. (2017). Time series analysis of total suspended solid (TSS) using Landsat data in Berau Coastal Area, Indonesia. International Journal of Remote Sensing and Earth Sciences (IJReSES), 14(1): 61-70. https://doi.org/10.30536/ijreses.v14i1.13957

[12] Abdelal, Q., Assaf, M.N., Al-Rawabdeh, A., Arabasi, S., Rawashdeh, N.A. (2022). Assessment of Sentinel-2 and Landsat-8 OLI for small-scale inland water quality modeling and monitoring based on handheld hyperspectral ground truthing. Journal of Sensors, 19: 4643924. https://doi.org/10.1155/2022/4643924

[13] Adjovu, G.E., Stephen, H., James, D., Ahmad, S. (2023). Overview of the application of remote sensing in effective monitoring of water quality parameters. Remote Sensing, 15(7): 1983. https://doi.org/10.3390/rs15071938

[14] Pratiwi, F.K.W.N., Maslukah, L., Sugianto, D.N. (2022). Water quality and sediment at the mangrove information center (PIM), Pekalongan (in Indonesian). Indonesia Journal of Oceanography (IJOCE), 4(3): 33-43. https://doi.org/10.14710/ijoce.v4i3.14141

[15] Izzaty, A., Ramli, I., Bakri, B. (2026). Water quality estimation from total suspended solid and dissolved oxygen concentration in Krueng Pase Watershed, North Aceh, Indonesia. International Journal of Environmental Impacts, 9(1): 62-73. https://doi.org/10.56578/ijei090106

[16] Arafah, F., Taufik, M., Jaelani, L.M. (2015). Analysis of seawater quality parameters in the waters of Sumenep Regency for mapping the distribution of pelagic fish potential (Case study: Total suspended solids (TSS)). In Proceedings of the National Conference on Regional Infrastructure Technology Applications (ATPW). https://doi.org/10.13140/RG.2.1.4871.8801

[17] Hamdan, A.M., Fajar, M.T., Wahid, M.A., Mustaqin, R., Maulana, R., Zainuddin, M.F. (2022). Monitoring of river estuary turbidity using satellite image analysis and its correlation to rainfall (A case study of the Krueng Aceh River, Indonesia). Jurnal Fisika Flux, 19(3): 222-235.

[18] Sinaga, M.P., Siburian, D.T.E., Zega, E.K. (2024). The impact of total suspended solid (TSS) and containing water chlorophyll-a on the fertility level of Jakarta Bay waters using technology of Google Earth Engine (GEE) clouds. Jurnal Ilmiah Platax, 12(2). https://agris.fao.org/search/en/providers/126017/records/6970b6cbbd789e57df2ced9e.

[19] Ramli, I., Achmad, A., Basri, H., Izzaty, A. (2022). Erosion and distribution of total suspended sediment (TSS) using Landsat-8 in Krueng Pase Watershed. In Proceedings of the Second International Conference of Construction, Infrastructure, and Materials, Springer Nature Singapore, pp. 23-33. https://doi.org/10.1007/978-981-16-7949-0_3

[20] Sent, G., Biguino, B., Favareto, L., et al. (2021). Deriving water quality parameters using Sentinel-2 imagery: A case study in the Sado Estuary, Portugal. Remote Sensing, 13(5): 1043. https://doi.org/10.3390/rs13051043